



University of  
Massachusetts  
Amherst

## Impacts of Global Warming of 1.5, 2.0 and 3.0 °C on Hydrologic Regimes in the Northeastern U.S.

Item Type	article
Authors	Siddique, Ridwan;Mejia, Alfonso;Mizukami, Naoki;Palmer, Richard N.
DOI	<a href="https://doi.org/10.3390/cli9010009">10.3390/cli9010009</a>
Rights	UMass Amherst Open Access Policy
Download date	2026-03-07 15:19:38
Item License	<a href="http://creativecommons.org/licenses/by/4.0/">http://creativecommons.org/licenses/by/4.0/</a>
Link to Item	<a href="https://hdl.handle.net/20.500.14394/5399">https://hdl.handle.net/20.500.14394/5399</a>

## Article

# Impacts of Global Warming of 1.5, 2.0 and 3.0 °C on Hydrologic Regimes in the Northeastern U.S.

Ridwan Siddique<sup>1,\*</sup>, Alfonso Mejia<sup>2</sup>, Naoki Mizukami<sup>1</sup> and Richard N. Palmer<sup>3</sup>

<sup>1</sup> Research Applications Laboratory, National Center for Atmospheric Research, P.O. Box 3000, Boulder, CO, USA; mizukami@ucar.edu

<sup>2</sup> Department of Civil and Environmental Engineering, Pennsylvania State University, University Park, PA 16802-1408, USA; amejia@engr.psu.edu

<sup>3</sup> Department of Civil and Environmental Engineering, University of Massachusetts, Amherst, MA 02115, USA; rpalmer@engin.umass.edu

\* Correspondence: ridwan.siddique@gmail.com; Tel.: +1-817-987-7967

**Abstract:** Regional climate change impacts show a wide range of variations under different levels of global warming. Watersheds in the northeastern region of the United States (NEUS) are projected to undergo the most severe impacts from climate change in the forms of extreme precipitation events, floods and drought, sea level rise, etc. As such, there is high possibility that hydrologic regimes in the NEUS may be altered in the future, which can be absolutely devastating for managing water resources and ecological balance across different watersheds. In this study, we present a comprehensive impact analysis using different hydrologic indicators across selected watersheds in the NEUS under different thresholds of global temperature increases (1.5, 2.0 and 3.0 °C). Precipitation and temperature projections from fourteen downscaled Global Circulation Models (GCMs) under the representative concentration pathway (RCP) 8.5 greenhouse gas concentration pathway are used as inputs into a distributed hydrological model to obtain future streamflow conditions. Overall, the results indicate that the majority of the selected watersheds will enter a wetter regime, particularly during the months of winter, while flow conditions during late summer and fall indicate a dry future under all three thresholds of temperature increase. The estimation of time of emergence of new hydrological regimes show large uncertainties under 1.5 and 2.0 °C global temperature increases; however, most of the GCM projections show a strong consensus that new hydrological regimes may appear in the NEUS watersheds under 3.0 °C temperature increase.

**Keywords:** GCMs; climate change; hydrologic modeling; time of emergence; hydrologic regimes



**Citation:** Siddique, R.; Mejia, A.; Mizukami, N.; Palmer, R.N. Impacts of Global Warming of 1.5, 2.0 and 3.0 °C on Hydrologic Regimes in the Northeastern U.S. *Climate* **2021**, *9*, 9. <https://doi.org/10.3390/cli9010009>

Received: 5 December 2020

Accepted: 1 January 2021

Published: 7 January 2021

**Publisher's Note:** MDPI stays neutral with regard to jurisdictional claims in published maps and institutional affiliations.



**Copyright:** © 2021 by the authors. Licensee MDPI, Basel, Switzerland. This article is an open access article distributed under the terms and conditions of the Creative Commons Attribution (CC BY) license (<https://creativecommons.org/licenses/by/4.0/>).

## 1. Introduction

Decision making in many areas of water resources is becoming increasingly challenging due to climate change and other anthropogenic activities [1–4]. Changing climate and increased warming of the atmosphere are expected to alter the regional hydrological cycle throughout the world, posing many adverse consequences to different sectors of society (e.g., agriculture, ecosystems, hydropower, navigation and water supply) [5]. The northeastern region of the United States (NEUS) has been projected to be highly vulnerable to climatic changes [6–8]. In particular, water resources and forest ecosystems in the NEUS show close sensitivity to weather and climate dynamics. Warming of the climate and changes in precipitation pattern can threaten the subtle balances between the NEUS' earth subsystems by changing the characteristics of seasonal streamflow patterns and river ice dynamics, timing of spring runoff, degree of evapotranspiration and snow depth, soil moisture and climate extremes (i.e., floods and droughts). This means that climate change can adversely impact hydrological regimes to add more complexity in water management across the NEUS [9].

In December 2015, the 21st Annual Conference of Parties (COP21) was held in Paris, which is also popularly known as the 2015 Paris Climate Conference. In the conference, the participating nations (more than 180 of them) from all around the world negotiated an agreement on the reduction in climate change impacts, calling for necessary actions to limit any future increase in global mean temperature (GMT) to well below 2 °C above pre-industrial levels and to pursue efforts to restrict it to 1.5 °C [10]. Such targets for minimizing global warming were put forward to significantly reduce the risks and impacts of climate change. However, they seem to be overly ambitious at this point of time considering the current policies and future national plans that were submitted by different countries in preparation of the 2015 Paris agreement to reduce greenhouse gas (GHG) emission [11].

Through Intended Nationally Determined Contributions (INDCs), different countries have spelled out their future targets to restrict GHG emissions, while some countries have also proposed conditional INDCs by mentioning a range of reduction targets. The collective implementation of all INDCs will still lead to a median warming of 2.6–3.1 °C in the 21st century, which is much higher than the targets of 2015 Paris agreement. Due to differences in mitigation strategies and uncertainties regarding future GHG emission policies, it remains unclear whether a 1.5, 2 or 3 °C change in global warming levels can be achieved [12]. Therefore, scientists and policy makers in many parts of the world have urged for increased understanding of the possible consequences under different global warming levels [13]. Additionally, regional warming rates are different to global warming rates, which could lead to diverging climate trends at the regional scale. For these reasons, regional climate change impacts to our natural and built environment and their associated uncertainties need to be investigated at various levels of global warming. This could provide regional stakeholders with enough quality information to use as guidance for improved policy making and adaptation measures at various stages in the future.

In hydrology, regional climate change studies have thus far been focused on differences between historical and future time periods [6,14,15]. For instance, many of these studies discuss how climate change impacts (i.e., floods or droughts, precipitation, temperature, runoff, streamflow, etc.) will change through a future time period, such as 2071–2100, compared to a base period in the past under different emission scenarios or representative concentration pathways (RCPs) [8,16,17]. While RCPs are useful for understanding the risks associated with emission scenarios, they have limitations in determining differences at different warming levels (2 or 3 °C) [18]. Within the Coupled Model Intercomparison Project (CMIP) experiment, it is sometimes challenging to understand whether anomalies between time periods are due to enhanced global warming or some other driving factor. However, recent studies after the Paris agreement have shifted their focus more towards different warming levels.

Karmalkar and Bradley (2017) have shown that the NEUS will be warming at a much faster rate in the 21st century than many other regions in the Contiguous United States (CONUS). This fast warming trend is likely to impact regional hydrological features, especially in the areas where river runoffs are dominated by snow accumulation and melting processes [19]. It is possible that due to increased warming, there will be less precipitation in the form of snow, evaporative demand will increase and snowmelt will occur earlier than usual. The cumulative effect of all these outcomes in the future can alter the timing of spring runoff and many other seasonal trends.

Hydrological studies that have explicitly utilized Global Circulation Model (GCM) projections to predict future streamflow conditions have already shown increases in seasonal streamflow and winter floods across the NEUS [7,14,15]. While the outcomes of many of these regional studies are more or less consistent, there is, however, a lack of consensus among GCM projections regarding possible timelines of these future impacts or when in the future these changes are likely to take place. More importantly, it needs to be investigated how alterations in regional streamflow conditions and hydrological regimes are associated with different warming levels [20,21]. Such studies are also useful

to highlight potential local or regional consequences that can be avoided by limiting global warming by 1.5 or 2 °C above pre-industrial levels.

In this study, we provide a comprehensive impact analysis on different hydrological indicators in the NEUS at different global warming levels of 1.5, 2 and 3 °C. We use downscaled climate projections from 14 GCMs to make an ensemble of hydrological simulations from a physically-based distributed hydrological model. Our main goal here is to obtain a robust understanding of the possible regional consequences under different global warming levels. Particularly, we explore whether there are any significant differences in climate change impacts for streamflow conditions across different spatiotemporal scales.

## 2. Study Area

NEUS is one of the more densely populated regions in the United States. As such, the majority of watersheds are under the influence of heavy anthropogenic activities, i.e., water regulations, land use and land cover changes, population growth, etc. Climate variabilities in combination with anthropogenic activities may act as a threat to flow regimes in the NEUS watersheds. In this study, we have selected eight different watersheds with different land use and land cover types to investigate future flow regimes. These eight selected watersheds are among the least regulated watersheds of NEUS having basin areas between 12.2 and 387.16 km<sup>2</sup>. We selected the least regulated watersheds in order to facilitate a more accurate calibration of the hydrological models (Figure 1). At regulated sites, flow conditions are generally altered and observations merely reflect natural flow conditions. In Table 1, we provide brief descriptions of the watersheds that have been examined in this study.

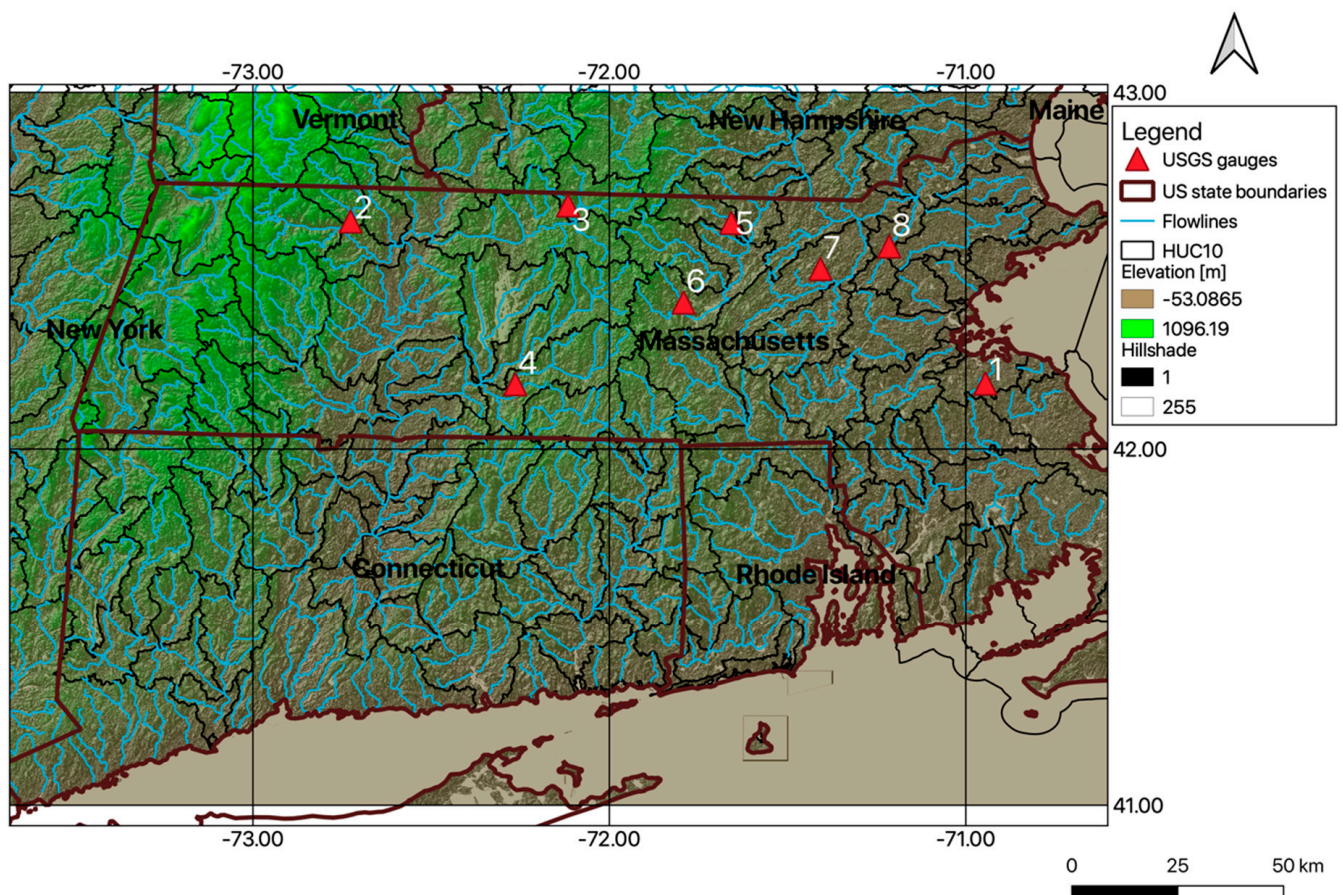


**Figure 1.** Study watersheds selected in the NEUS.

**Table 1.** Descriptions of selected watersheds within northeastern region of the United States (NEUS).

No.	USGS ID	Location	Area (km <sup>2</sup> )	Lat/Lon	Land Use
1	01105600	Old Swamp River, MA	12.2	42°11'25" 70°56'43"	Forest, 41%; residential, 34%
2	01169000	North River at Shatteckville, MA	230.69	42°38'18" 72°43'32"	Forested
3	01162500	Priest Brook near Winchedon, MA	49.70	42°40'57" 72°06'56"	Mostly forested
4	01176000	Quaboag River near West Brimfield, MA	387.16	42°10'56" 72°15'51"	Forested
5	01096000	Squannacook River near West Groton, MA	173.14	42°38'03" 71°39'30"	7.3% imperviousness, 18% permanently protected land area
6	01095220	Stillwater River near Sterling, MA	78.69	42°24'39" 71°47'30"	Mostly undeveloped forest and wetlands
7	01097380	Nasoba Brook near Acton, MA	33.17	42°30'45" 71°24'17"	25% protected open space, 10% impervious
8	01100600	Shawsheen River near Wilmington, MA	96.42	42°34'05" 71°12'55"	50% residential, 30% forest

### 3. Dataset

#### 3.1. GCM and Downscaled Output

The set of 14 climate models used in this hydrological modeling effort was selected from the Coupled Model Intercomparison Project Phase 5 (CMIP5; Taylor et al. 2012 [22]) ensemble of 36 models under two scenarios: RCP8.5 and RCP4.5 [23]. The CMIP5 ensemble of 36 climate models (GCMs) and 4 different scenarios (RCP8.5, RCP6.0, RCP4.5 and RCP2.6) captures any of the uncertainties in projections (though the ensemble is not systematically designed for the purpose). While it is ideal to use all available data in production of climate change projections, a careful evaluation of these models is necessary to establish their credibility in providing reliable climate information for the region of interest. The ensemble may also contain redundant information on projections. By combining information on model performance and similarities in their projections, it is possible to reduce the size of the ensemble without losing critical climate change information.

In this study, we only use a subset of the CMIP5 models (14) that were carefully selected for studies of climate impacts in the northeastern U.S. The framework used for their selection is described in detail in Karmalkar et al. [24] and is based on original coarse-resolution GCM data. The model selection involves a thorough assessment of the model performance of 36 CMIP5 models to evaluate their ability to capture key climate features of the northeastern U.S. including temperature and precipitation climatology, the annual cycle, variability and large-scale circulation, facilitating the selection of 10–15 models. The subset of selected models adequately captures the uncertainty in temperature and precipitation projections seen across 36 CMIP5 models and represents diversity in the spatial patterns of precipitation projections.

Regional projections for the Commonwealth of Massachusetts are produced using the downscaled counterparts of the selected models: the Localized Constructed Analogs (LOCA) downscaled dataset [25]. This is a statistical downscaling method [25] that relies on selecting appropriate analog days from observations to downscale coarse-resolution GCM data to finer spatial scales. The LOCA downscaling method has been shown to improve depiction of precipitation extremes over the previous statistical downscaling (e.g., BCSD) methods [25]. The LOCA dataset is available at 6-km resolution.

### 3.2. Observed Meteorological and Streamflow Data

We used multi-sensor precipitation estimates (MPEs) as the observed precipitation data for hydrological model calibration and validation runs. MPEs are produced hourly through the optimal combination of multiple radars and hourly rain gauge data at  $4 \times 4 \text{ km}^2$  grid resolution [26]. The MPE product used was obtained from the NOAA's Northeast River Forecasting Center (NERFC) and is similar to the National Centers for Environmental Prediction (NCEP) stage IV MPEs [27,28]. Gridded MPE products are now widely used in different hydrometeorological applications [29,30]. The hydrological model used in this study requires gridded temperature observations to obtain monthly potential evaporation and, as input to the SNOW-17 model, to determine snow accumulation and melt. The gridded temperature data were obtained from the NERFC, which generated the data by combining multiple observation networks (Meteorological Aerodrome Report, USGS stations and the NWS Cooperative Observer Program). All the gridded data used in this study were resampled using bilinear interpolation onto the regularly spaced grid ( $4 \times 4 \text{ km}^2$  cell size) required by the hydrological model. For the verification of the streamflow simulations, daily discharge data from the relevant USGS gauges were used. In total, thirteen years (2004–2016) of streamflow observations were used.

### 3.3. Determination of 1.5, 2.0 and 3.0 °C Time Periods

Different GCMs have different sensitivities to climate forcing and GHG emission scenarios. As such, timelines of mean global temperature increases of 1.5, 2.0 and 3.0 °C with respect to pre-industrial conditions will be different among GCMs due to their variations in model initializations, structures and parameterizations. In this study, we have calculated threshold crossing times (TCTs) for individual GCMs and a time sampling approach has been implemented [31]. This time sampling method has been widely used in other studies as well [21,32,33]. A twenty-year running mean global temperature is compared to those of the 1981–2000 period in the GCM simulations while 1981–2000 corresponds to a 0.9 °C temperature increase with respect to pre-industrial conditions [34]. The first 20-year period with global warming crossing one of the three warming levels (1.5, 2.0 and 3.0 °C) is then determined for each of the 14 GCMs under the RCP8.5 emission scenario. Different hydrologic indicators are estimated across the threshold crossing times to understand the impact of different levels of global warming on hydroclimatic conditions, and later, they were compared with a base period (1980–1999). The identified 20-year time period for the corresponding GCM is shown in Table 2.

**Table 2.** Timelines for Global Circulation Models (GCMs) to reach different levels of thresholds of temperature increases in the NEUS.

Model	1.5 °C	2.0 °C	3.0 °C
MPI-ESM-LR	2012–2031	2030–2049	2058–2077
HadGEM2-ES	2020–2039	2028–2047	2049–2068
CMCC-CMS	2023–2042	2025–2044	2053–2072
MPI-ESM-MR	2015–2034	2023–2042	2053–2072
inmcm4	2038–2057	2050–2069	2078–2097
CanESM2	2009–2028	2022–2041	2043–2062
GFDL-ESM2G	2037–2056	2053–2072	2078–2097
bcc-csm1-1-m	2014–2033	2029–2048	2056–2075
IPSL-CM5A-LR	2009–2028	2023–2042	2043–2062
GISS-E2-R	2027–2046	2047–2066	2080–2099
HadGEM2-CC	2015–2034	2031–2050	2050–2069
CESM1-BGC	2009–2028	2025–2044	2051–2070
bcc-csm1-1	2016–2035	2028–2047	2053–2072
CESM1-CAM5	2022–2041	2034–2053	2049–2068

## 4. Methodology

### 4.1. Hydrological Modeling

The hydrological model selected for this work is NOAA's Hydrology Laboratory Research Distributed Hydrologic Model (HL-RDHM) [35], where the basin is divided into regularly spaced square grid cells to account for spatial heterogeneity and variability of geophysical conditions. Within the HL-RDHM, the heat transfer version of the Sacramento Soil Moisture Accounting model (SAC-HT) is employed for rainfall-runoff generation, as well as the SNOW-17 model to account for snow accumulation and melting. The SAC-HT is a process-based model of the system (conceptual) type which computes the freeze-thaw of soil moisture as well as evapotranspiration based on soil temperature [36]. The SNOW-17 model uses near-surface temperature to differentiate between snow accumulation or rain at each grid cell and generates snowmelt runoff. The runoff generated at each cell is routed through channel and stream networks using hillslope and kinematic wave routing. Overall, a fully distributed HL-RDHM has been implemented at  $2 \times 2 \text{ km}^2$  spatial resolution. This particular hydrologic model has been widely applied [37–39]. The model is fully described in [40].

The hydrological model was calibrated separately at each of the eight watersheds. Model calibration in the NEUS watersheds was a challenge since most of the watersheds in Massachusetts and surrounding states are highly regulated upstream. In total, there are more than 1400 dams in the Commonwealth, among which 53 are large, and as a consequence, both high and low flows are impacted. Due to such regulations, it was difficult to identify unregulated USGS stream gauges to calibrate the model. For this study, a very careful selection was made to identify eight Hydrologic Unit Code-8 (HUC-8) watersheds that are least regulated based on the existing reports and published documents [41,42]. In this process, an expert opinion was solicited from USGS. After selecting appropriate sites, the model parameters were calibrated at the selected locations using an automatic calibration technique called the "Stepwise Line Search" (SLS) over a period of 7 years (2004–2010) after making manual adjustments. Kuzmin et al. [43] describe the SLS technique in detail.

To assess the model performance, we used the following metrics: the correlation coefficient (R), percent bias (PB) and Nash–Sutcliffe efficiency (NSE). Model performance was measured using two different flow conditions: low to moderate flows and high flows. The former represents flows smaller than the 25th percentile of the overall flow distribution while the latter represent flows greater than 90th percentile. Through the validation process, it was found that the NSE value for most cases ranges between 0.55 and 0.80. Besides, PB, for most cases, ranges between 5 and 15 percent in the sense of absolute value. The range of correlation coefficient varies between 0.75 and 0.95, which can be considered a high standard for a physically-based hydrological model. In Table 3, we present the statistics of our calibrated model performance during the validation period.

**Table 3.** List of model calibration sites and validation statistics for annual mean flow.

No.	USGS ID	Location	NSE	KGE	PB
1	01105600	Old Swamp River, MA	0.68	0.61	8.76%
2	01169000	North River at Shatteckville, MA	0.72	0.65	12.30%
3	01162500	Priest Brook near Winchedon, MA	0.63	0.57	13.10%
4	01176000	Quaboag River near West Brimfield, MA	0.69	0.66	6.23%
5	01096000	Squannacook River near West Groton, MA	0.59	0.62	10.38%
6	01095220	Stillwater River near Sterling, MA	0.78	0.71	3.48%
7	01097380	Nasoba Brook near Acton, MA	0.58	0.52	15.62%
8	01100600	Shawsheen River near Wilmington, MA	0.56	0.62	9.72%

### 4.2. Hydrologic Flow Conditions

Anomalies in mean annual flows across TCTs (listed in Table 2) with respect to long-

term mean annual discharge under different thresholds of temperature increases were calculated using the following equation:

$$\text{Anomaly} = (Q_i - Q_m) / \sigma, \quad (1)$$

where  $Q_i$  is the annual discharge (mm/WY) in year  $i$ ;  $Q_m$  is the long-term mean annual discharge (mm/WY); and  $\sigma$  is the standard deviation (mm/WY). For this study, the three distinct hydrologic flow conditions of dry (anomaly  $< -0.5$ ), average ( $-0.5 < \text{anomaly} < 0.5$ ) and wet (anomaly  $> 0.5$ ) years were established based on discharge anomaly.

#### 4.3. Hydrological Indicators

As hydrological indicators, we investigated future changes in magnitude, timing and frequency of mean monthly flow and high and low flows. Mean monthly flows are indicative of available water resources, e.g., for agriculture, water supply, navigation, etc., while high and low flows are indicative of wet and dry conditions, respectively.

#### 4.4. Estimation of Time of Emergence

Climate can change due to both internal and external factors. Internal climate change factors generally include naturally occurring processes such as ocean–atmosphere interactions, atmospheric equilibrium and unchanging trends of temperature during pre-industrial times. This type of variation in climate can be termed as internal climate variation (ICV). On the contrary, external climate change factors include GHG emissions, anthropogenic land use and land cover changes, etc., which are also known as human-induced climate change (HICC) factors. The impact of ICV on climate change has been widely discussed in recent literature [44–47] and it has been found that ICV will play a significant role in local and regional climate projections, especially in the near term (for the years 2010–2060). Many studies have also compared the roles of HICC factors and ICV in future change projections [20,48–50]. While investigating the relative roles of ICV and HICC on future climate change, Hawkins and Sutton [48] have identified a process to estimate time when the role of HICC becomes greater than ICV and decided to term it as “Time of emergence” or ToE. In this study, we have considered ICV as multi-decadal variability and estimated ToE over a period of 20 years. Our methodology to estimate ToE is similar to what has been described in Zhuan et al. (2018), except that we have decided to use outputs from one GCM out of fourteen, which gives us the median changes for annual mean streamflow across the years 1980–2099 while Zhuan et al. used the ensemble mean of 40 different GCMs to demonstrate the ToE. In this study, we have used a single GCM (GISS-E2-R) to determine the ToE since we wanted to demonstrate the effect of different temperature increases, and this can only be done for individual model outputs, not for the mean of a model ensemble. Here, we selected GISS-E2-R because it tends to provide the median estimate of future streamflow conditions across selected watersheds. Below we describe the step-by-step procedure to estimate ToE:

1. Using each of the 14 model simulations for the years 1980–2099, we estimated one hundred 20-year periods varying by one year, i.e., 1980–1999, 1981–2000, 1982–2001, . . . , 2080–2099.
2. The 20-year mean value was calculated for each period. A total of 100 mean values were obtained for each climate simulation.
3. The change in streamflow for each of 100 mean values relative to mean value at the reference period (1980–1999) was calculated
4. The median value of these changes, which was represented by the model GISS-E2-R over 14 simulations, was defined as HICC.
5. The standard deviation of the streamflow changes over members was calculated for each period and a total of 100 standard deviation values were obtained. ICV was then defined as  $\pm 2$  or  $\pm 1$  standard deviations of inter-member differences.

With the above steps, the 100 HICC values form a curve (GISS-E2-R model) and the ICV values form another curve, and the intersection of these two curves is defined as the ToE. If an HICC curve intersects an ICV curve of +2 or +1 standard deviations, it implies that there is an increasing climate change trend. If an HICC curve intersects an ICV curve of  $-2$  or  $-1$  standard deviations, then there is a decreasing climate change trend. No intersection implies that HICC does not emerge from ICV or that there is no obvious HICC.

## 5. Results

### 5.1. Changes in Precipitation

Mean areal precipitation in the selected basins of NEUS shows significantly different future trends under different thresholds of temperature increases. Climate change signals for different seasons are also found to be different. In Figure 2, we show climate change impacts on monthly mean precipitation from fourteen different GCM projections under 1.5, 2.0 and 3.0 °C temperature increases, where solid lines represent ensemble means of fourteen GCMs and the shaded region represents the region of model uncertainty. Future projections in winter months (Dec–Feb) show increases in precipitation under all three thresholds of temperature increase. The largest increases in precipitation during winter are shown under the scenario of the 3.0 °C temperature increase which varies between 5 and 24 percent among different GCMs. Precipitation increases approximately similarly for 1.5 and 2.0 °C, which is around 2~12 percent, although the ensemble mean of fourteen models suggest slightly greater increases for 2.0 °C when compared to increases for 1.5 °C. Increases in the precipitation amount during winter may include increases both in liquid rain and snow since GCM projections have shown that number of days above 0 °C will increase in the future across the NEUS [7]. Thus, different levels of temperature increase in combination with increased heavy precipitation events in the future may significantly impact winter peak flows in NEUS watersheds.

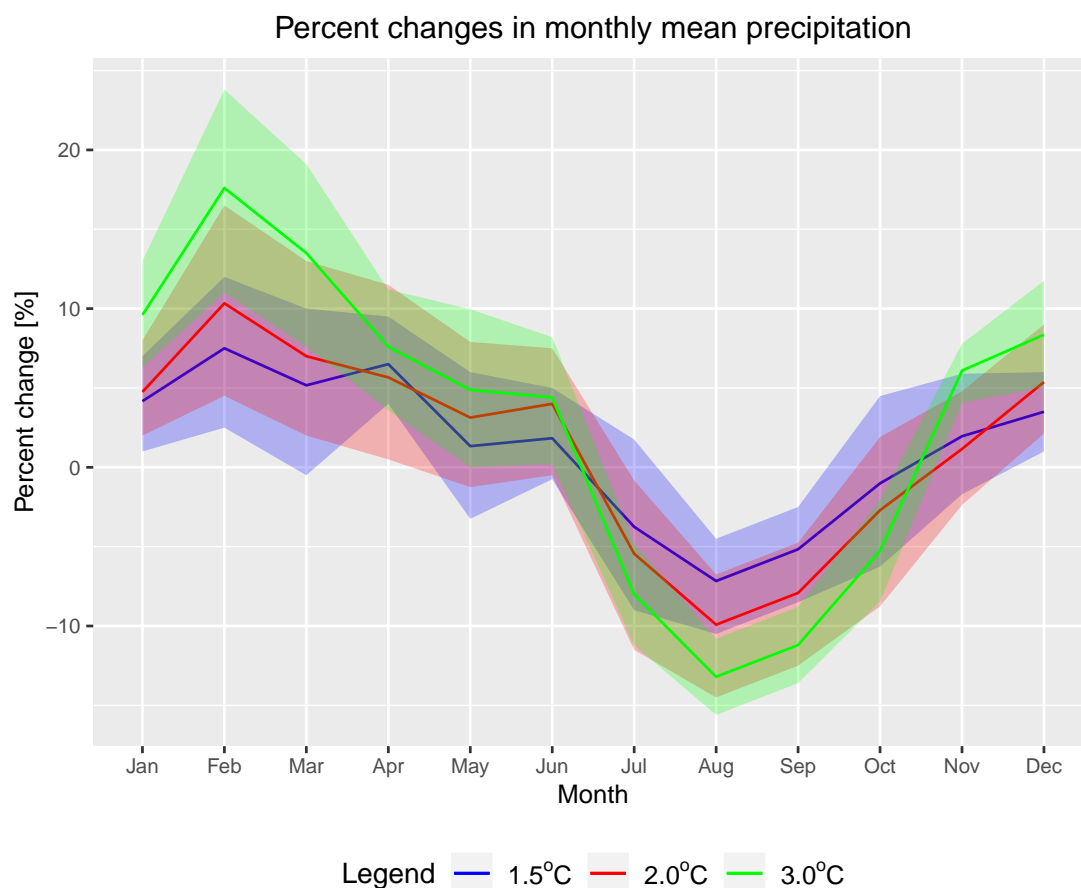


**Figure 2.** Percent changes in daily mean of monthly precipitation across all eight basins under different levels of temperature increases relative to the base period (1980–1999).

During spring months (Mar–May), the majority of the GCM projections show increases in precipitation, except a few. The range of precipitation increases during spring projected by different GCMs under different warming levels are shown to be approximately similar and ranges between  $-2$  and  $13$  percent for different watersheds. The results in Figure 2 also indicates that summer (Jun–Aug) can be the driest season of the year in terms of future decreases in precipitation. Specifically, the greatest decreases in precipitation are projected during the months of July and August under the  $3.0$  °C increase in temperature. The ensemble mean of GCM projections suggests that decreases are slightly less prominent for the  $1.5$  and  $2.0$  °C scenarios, although all fourteen GCMs indicate the same climate change signal of decreasing precipitation trends during summer months, except June.

Decreases in precipitation are also shown during fall (Sep–Nov), especially during the earlier part of the season. However, the model ensemble mean suggests that decreases are slightly smaller compared to summer months and range between  $-2$  and  $-12$  percent. Overall, future trends of precipitation under different levels indicate a significant increase in precipitation during winter and spring. Precipitation is projected to decrease across NEUS watersheds during late summer and the earlier months of fall. These change projections in precipitation should have an impact on future flow regimes in the NEUS and adjacent areas.

## 5.2. Changes in Streamflow Conditions

### 5.2.1. Magnitude

In this section, we will discuss the impact of climate change on flow regimes in the NEUS, which is evaluated for different thresholds of temperature threshold of  $1.5$ ,  $2$  and  $3$  °C. First, mean changes in climatic driving forces are presented to differentiate the causes of change in each of the basins. In Figure 3, we show percent changes in the daily mean of monthly flow across all basins for different thresholds of temperature increase. Solid lines represent the mean changes and the shaded regions represent the changes from fourteen GCMs and across all eight basins that have been considered in our study. Apparently, future trends for monthly flows are found to be consistent for different temperature increases. For instance, the monthly flow in winter months (December–February) has shown consistent increases for all three thresholds of temperature increase ( $1.5$ ,  $2.0$  and  $3.0$  °C). These increases in monthly flows can be the direct influence of potential future increases in winter precipitation. With increased temperature, there will be increased precipitation more in the form of rain than snow. Increased rain events in combination with snowmelt runoff may influence the winter peak flows to rise more in the future compared to the present. Our results in Figure 3 also confirm the same trends where the  $3.0$  °C temperature increase shows greater increases in winter flows when compared to the  $1.5$  and  $2.0$  °C temperature thresholds. For the  $3.0$  °C temperature threshold, increases in winter flow range between  $25$  and  $75$  percent across all watersheds, while the  $2.0$  and  $1.5$  °C increases show ranges between  $5$  and  $30$  percent and  $0$  and  $30$  percent, respectively. The greatest increases in winter peak flows are shown during the month of February for all three temperature thresholds.

In NEUS watersheds, peak flows generally occur during the month of March or April when snowmelt is triggered by increased temperature. In the future, however, spring runoff exhibits a decreasing trend, particularly during the month of April. This can be the consequence of earlier snowmelt than normal due to a rise in temperature level. More specifically, temperature increases in the future will cause a shift in the timing of spring runoff, which indicates that snowmelt runoff will more likely start around March instead of April, and therefore, there will be increases in monthly flows of March but decreases will occur during April. The magnitudes of changes in April floods are shown to be similar for different thresholds of temperature increases and they range around  $-5$ – $-15$  percent across all basins.

Flows during the summer months have shown mixed results when most of the watersheds across all temperature thresholds have shown small increases in flows, particularly for the month of June. However, as time increases in summer, more and more watersheds

start to show decreases in flows. The mean changes across all basins show maximum decreases during the month of August, especially for 1.5 and 2.0 °C temperature thresholds. This flow behavior during the months of summer can largely be associated with antecedent soil moisture. Since precipitation is projected to increase during winter and spring, there should be increased amounts of soil moisture which may persist through the earlier part of summer, helping base flows to exhibit slight increases despite increasing evaporative demand. As antecedent soil moisture starts to perish due to increased temperature, summer flows starts to show decreases towards the latter half of the season (during the months of July and August).

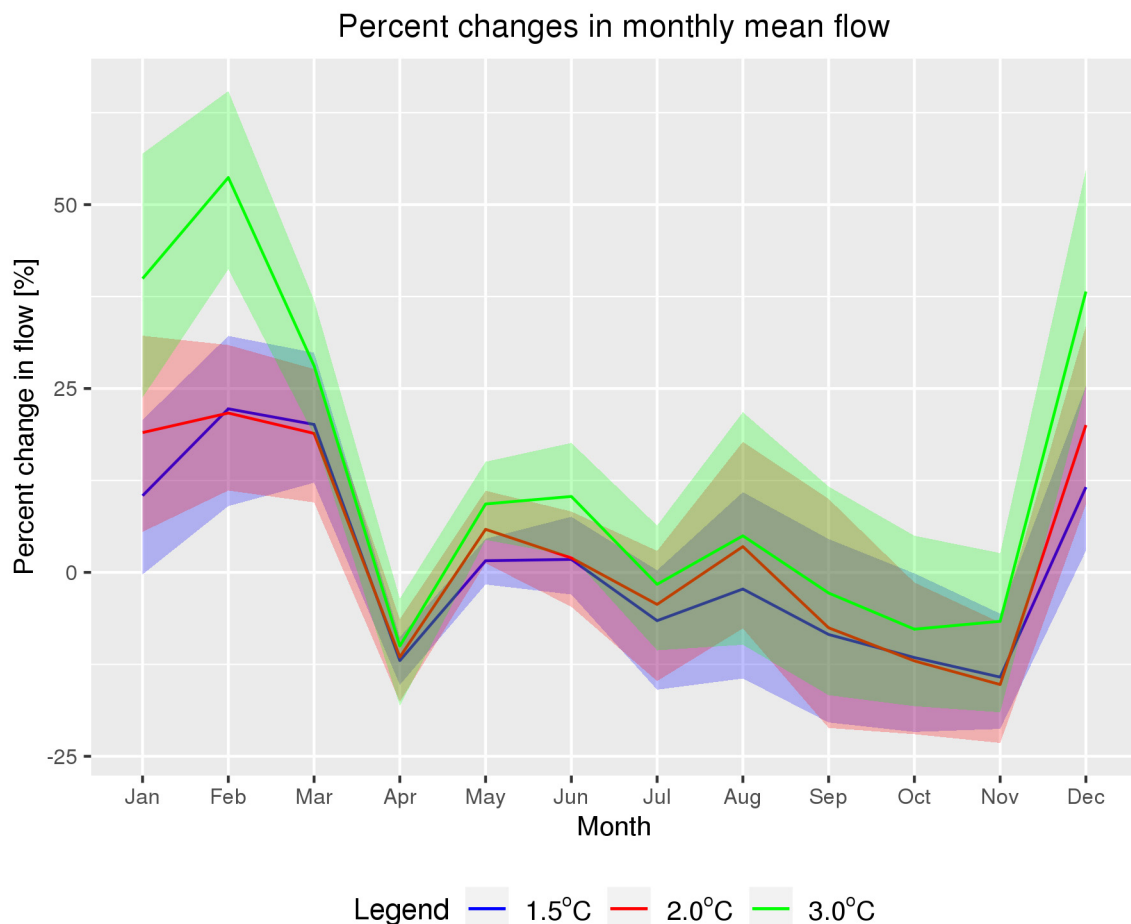


**Figure 3.** Percent changes in daily mean of monthly streamflow conditions under different levels of temperature increase relative to the base period (1980–1999).

Maximum decreases in monthly flows are observed during the months of fall (September–November) when approximately all our study watersheds are found to be getting drier for all three thresholds of temperature increases. These decreases range between 2 and 23 percent which shows the effect of lack of precipitation and increases in number of consecutive dry days during spring in the future [7]. This also indicates the possibilities of extended droughts in the northeastern watersheds during late summer and early part of the fall in the future.

### 5.2.2. Frequency

In Figure 4, we show the timing and frequency of annual peak flows reported by different GCMs under three different thresholds of temperature increase in the future. These outcomes under three thresholds of temperature increase are compared with the outcomes across a base period (for the years 1980–1999). To obtain the results, we have

considered all the peak flows greater than the 95th percentile in the flow distribution for all fourteen GCMs.

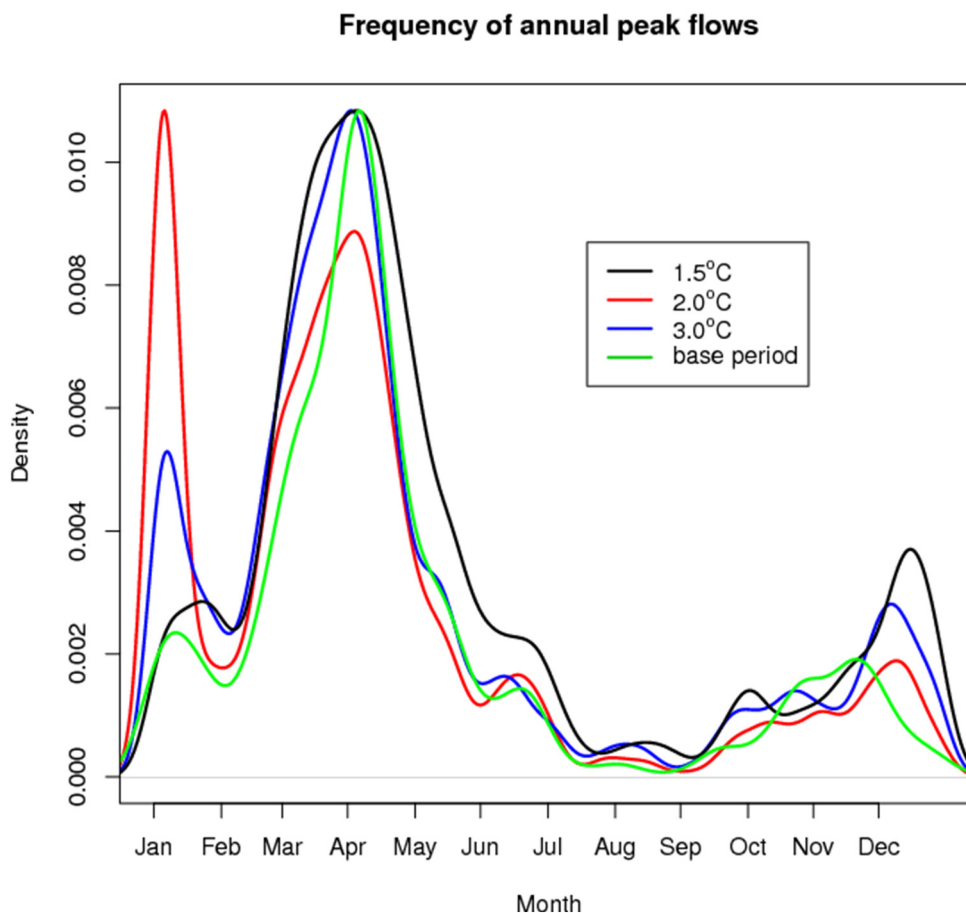


**Figure 4.** Probability distribution of the timing and frequency of annual peak flow events (above 95th percentile in the flow distribution) under different levels of temperature increase relative to the base period (1980–1999).

The results show clear indication of a few possible changes in the frequency and timing of peak flows in the eight different watersheds considered here. First, peak flows during the winter, particularly for the months of December and January, are shown to be increasing for all three thresholds of temperature increase (1.5, 2.0 and 3.0 °C). The maximum increases are shown for 2.0 °C increases in the month of January. However, increases are small during the month of February when compared to the base period. The results also show that maximum peak flows generally occur in the month of April during the base period, which will see a decrease in the future with increased temperature. On the contrary, the frequency of peak flows is also found to be increasing during the month of March. This is an indication that the frequency of peak flows will increase in the future during the months of winter and the early part of spring. With increased temperature, there will be increases in extreme precipitation and rain or snow events. The combination of increased rain and snowmelt, thus, may contribute to increases in the magnitude and frequency of runoff and streamflow peaks in the future.

### 5.3. Anomalies in Hydrological Flow Conditions

Figure 5 represents average anomalies for different temperature thresholds in the future compared to a base period (1980–1999). Since we used 14 different GCMs to understand uncertainties, we obtained 14 different realizations of hydrological flow anomalies for each basin. For the 1.5 °C temperature increase, the majority of the GCMs show anomaly values greater than 0.5, particularly for basins 2–5. An anomaly value over 0.5 means

that these basins will enter a wet regime for mean flow conditions compared to the base period. Two out of the eight basins (basins 1 and 6) show anomaly values around zero for most of the GCMs. This indicates that hydrological flow will remain the same and may not experience any major changes in the future. However, it should be noted that three to four GCMs also report anomaly values lower than  $-0.5$  for these two basins, which indicates a possible dry flow regime in the future. Since we consider each GCM output an equally likely scenario of the future, we should consider these results carefully as well. For the remaining two basins (basins 7 and 8), most of the anomaly values range between  $0.5$  and  $-0.4$ , which implies that average flow conditions will persist in these two basins. Anomaly results are shown to be almost similar for  $2.0\text{ }^{\circ}\text{C}$  temperature increases, which also indicate that more basins will enter a wet flow regime in the future when compared to the base period. The most extreme cases are found for  $3.0\text{ }^{\circ}\text{C}$  temperature increases when six out of eight basins, in the future, will experience a wetter flow regime. For these six basins, approximately 80 percent of the GCMs report anomaly values greater than  $0.5$ . The remaining two basins (basins 1 and 6) show anomaly values between  $0.5$  and  $-0.5$ , indicating average flow conditions (neither extremely dry nor wet) in the future. Overall, our results show that most of the basins in the U.S. northeast may undergo increases in flow conditions due to increased precipitation in this region. However, some GCMs also indicate a possible dry future for a few basins, especially in the seasons when precipitation is limited.

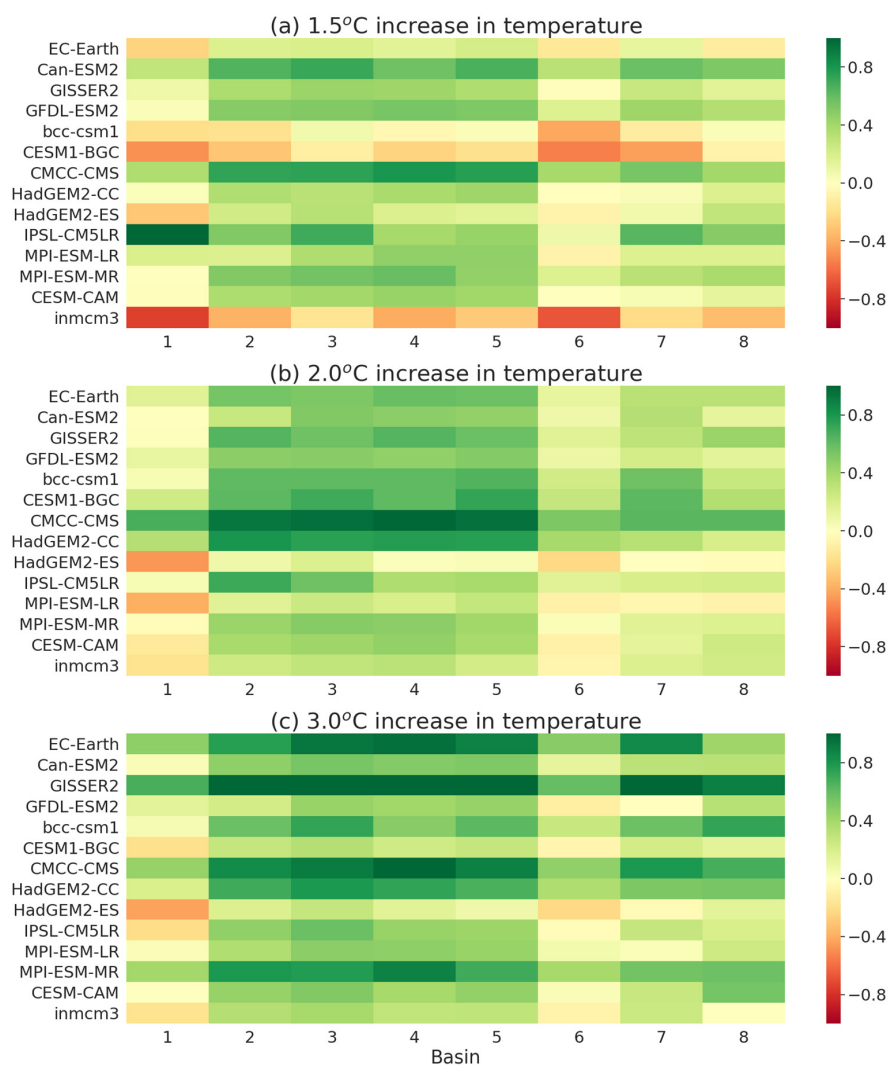


**Figure 5.** Average anomalies under different thresholds of temperature increases in the future compared to a base period (1980–1999).

#### 5.4. Alteration of Hydrologic Regimes

In Figures 6 and 7, we have shown the time of emergence for the annual mean streamflow for basins 1–4 and 5–8, respectively. Here, we have shown results for the GISS-E2-R model to illustrate regime changes across the years of 2000–2099. GISS-E2-R was chosen out of 14 GCMs because it demonstrates median changes for mean annual precipitation across Massachusetts. To produce conservation adaptation strategies, we have used both  $\pm 1$  standard deviation and  $\pm 2$  standard deviation as ICV. In Figures 6 and 7, the blue line represents HICC and the green and red dashed lines represent ICV of  $\pm 1$  standard deviation and  $\pm 2$  standard deviation, respectively. The intersection of the HICC and ICV curves represents the time of emergence of a new hydrological regime.

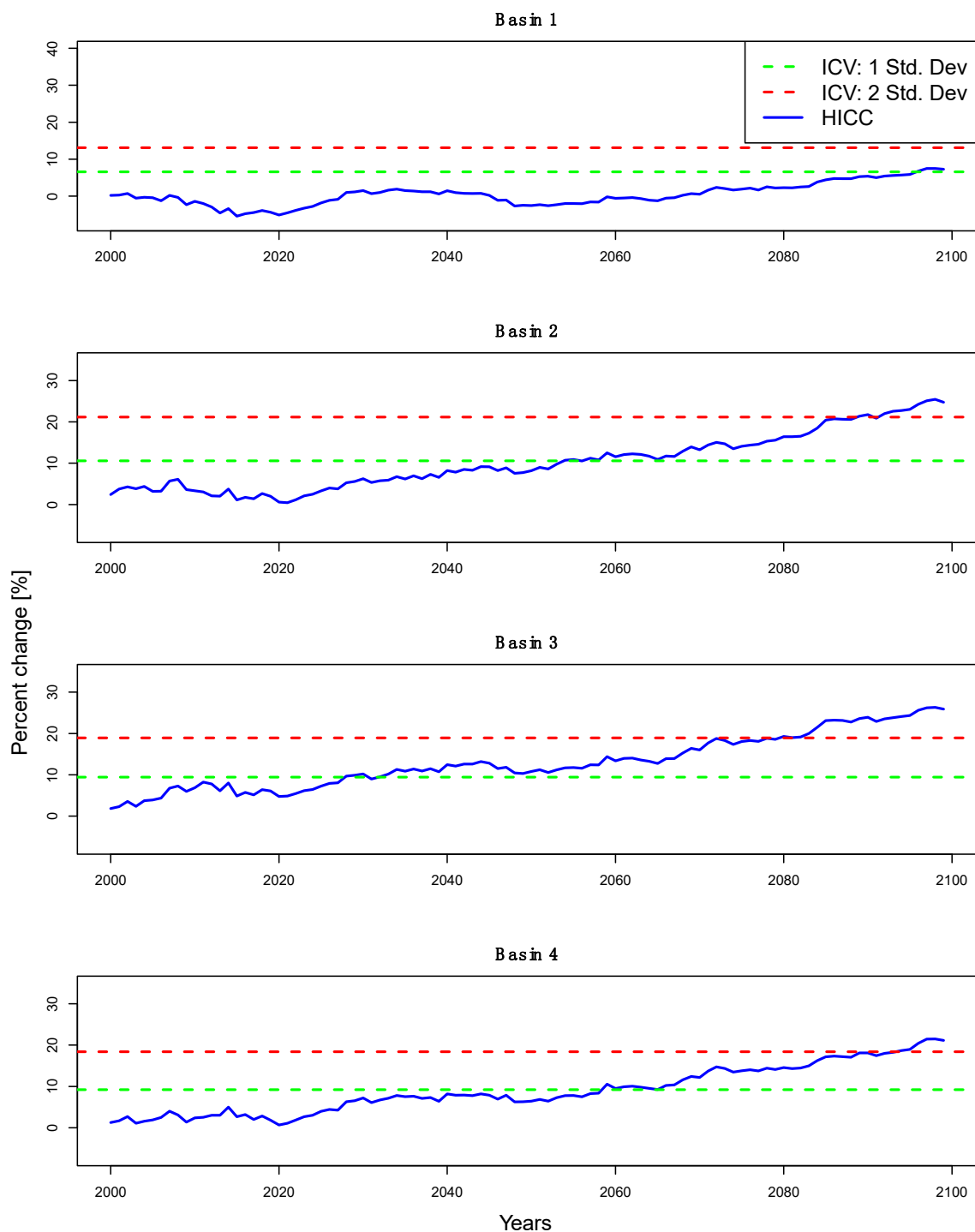


**Figure 6.** Time of emergence for mean annual streamflow conditions for watersheds (1–4).

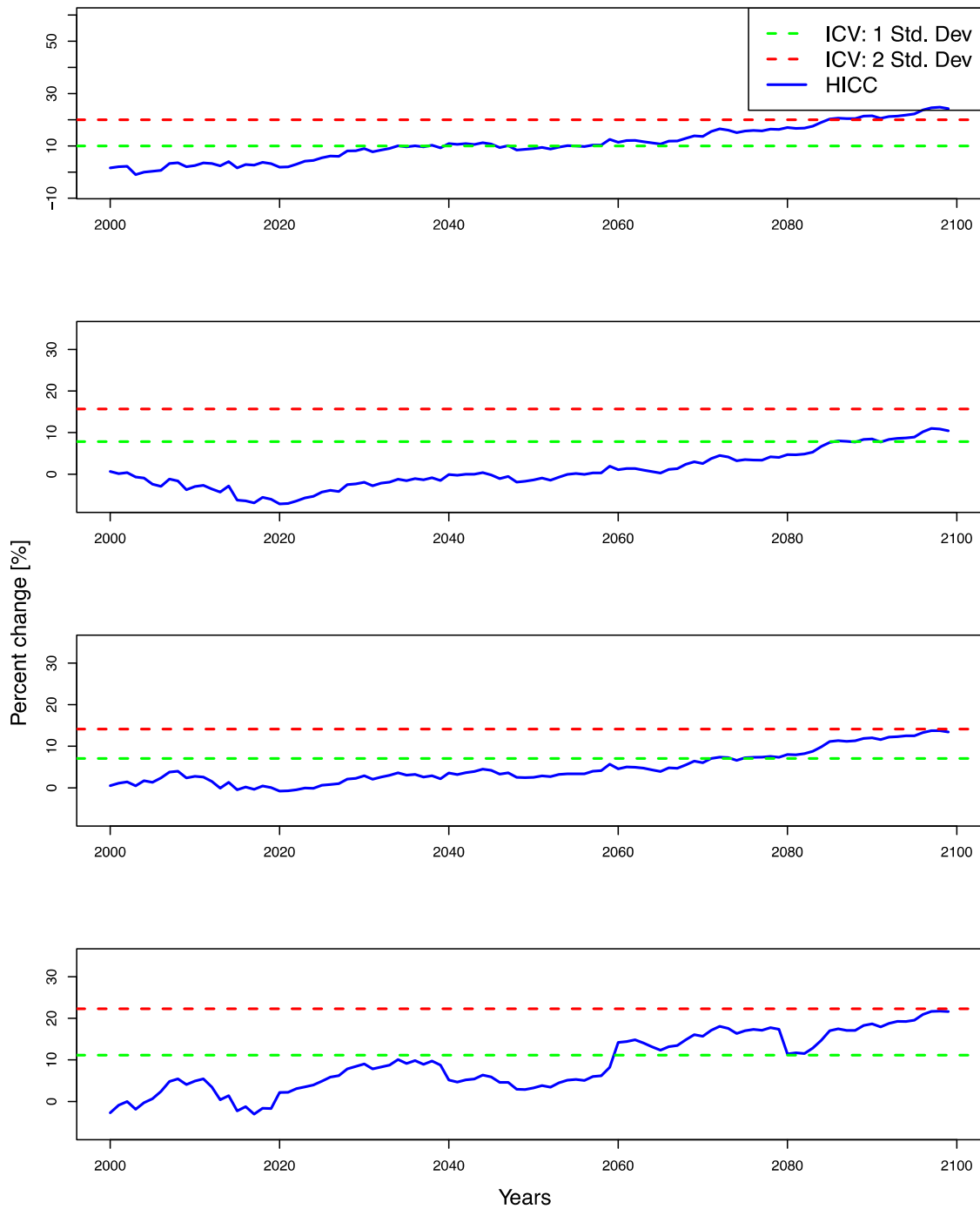


**Figure 7.** Time of emergence for mean annual streamflow conditions for watersheds (5–8).

The results in Figures 6 and 7 illustrate the emergence of new hydrological regimes for both ICV scenarios since the HICC curve crosses both ICV curves for 6 out of 8 basins, except for basins 1 and 6. However, Figures 6 and 7 cannot provide us with the impacts of different thresholds of temperature increase, which is the main focus of this study. For this reason, we have summarized the results of Figures 6 and 7 in Table 4, where we have used binary (yes/no) variables for basins 1–8 to represent whether new hydrological regimes will occur or not. In Table 4, we have also shown hydrologic regime changes for seasonal

mean flows across wet (Dec–May) and dry (Jun–Nov) seasons besides annual mean flow conditions. It is evident from results that there are uncertainties regarding ToE for the temperature thresholds of 1.5 and 2.0 °C for different flow conditions, although we are using a GCM that represent median changes. If we consider a more rigorous ICV of  $\pm 2$  standard deviation, none of the eight basins report hydrologic regime changes for the 1.5 and 2.0 °C temperature increases, and this trend is valid for all cases or flow conditions (wet, dry and annual). On the contrary, six out of eight basins (except basins 1 and 6) show regime changes for the 3.0 °C temperature increase, specifically for wet season and mean annual flow conditions. No hydrologic regime changes are found for dry seasons with ICVs of  $\pm 2$  standard deviation. For ICV of  $\pm 1$  standard deviation and annual mean flow, all eight basins considered here show regime changes for 3.0 °C, while six out of eight basins show regime changes with a 2.0 °C temperature increase. During the wet season,  $\pm 1$  standard deviation indicates a similar trend which indicates that most of the basins will undergo regime changes for all three thresholds of temperature increases in the future. In contrast, only few basins show regime changes during the dry season also for 3.0 °C temperature increases. Overall, the results indicate that most of the basins in the NEUS may enter a wetter regime, particularly with a 3.0 °C increase in global temperature. The median GCM projection also indicates that future hydrologic changes in the NEUS basins during dry periods may be less significant when compared to wet seasons. However, we should be aware that this finding may not be valid for the cases of extreme GCM projections. As  $\pm 2$  standard deviation is a more robust estimate and there is only a 2.3% chance to exceed it, we can say that a 3.0 °C temperature increase may have a strong influence on the emergence of a new hydrological regime in the watersheds of northeastern U.S.

**Table 4.** Summary chart showing whether or not time of emergence will occur under different levels of warming in the NEUS watersheds.

		ICV: 1 Std. Dev			ICV: 2 Std. Dev		
		1.5 °C	2.0 °C	3.0 °C	1.5 °C	2.0 °C	3.0 °C
Basin 1	Wet	Yes	Yes	Yes	No	No	No
	Dry	No	No	No	No	No	No
	Annual	No	No	Yes	No	No	No
Basin 2	Wet	Yes	Yes	Yes	No	No	Yes
	Dry	No	No	No	No	No	No
	Annual	No	Yes	Yes	No	No	Yes
Basin 3	Wet	Yes	Yes	Yes	No	No	Yes
	Dry	No	No	Yes	No	No	No
	Annual	Yes	Yes	Yes	No	No	Yes
Basin 4	Wet	Yes	Yes	Yes	No	No	Yes
	Dry	No	No	No	No	No	No
	Annual	No	Yes	Yes	No	No	Yes
Basin 5	Wet	Yes	Yes	Yes	No	No	Yes
	Dry	No	No	No	No	No	No
	Annual	Yes	Yes	Yes	No	No	Yes
Basin 6	Wet	No	No	Yes	No	No	No
	Dry	No	No	No	No	No	No
	Annual	No	No	Yes	No	No	No
Basin 7	Wet	Yes	Yes	Yes	No	No	Yes
	Dry	No	No	No	No	No	No
	Annual	No	No	Yes	No	No	Yes
Basin 8	Wet	No	Yes	Yes	No	No	Yes
	Dry	Yes	Yes	Yes	No	No	No
	Annual	No	No	Yes	No	No	Yes

## 6. Conclusions

For a better understanding of regional climate change impacts and adaptation planning, we need studies targeting local consequences from different levels of global warming. In this study, we used climate projections from 14 carefully selected GCMs to force a physically-based distributed hydrological model to understand future changes in hydrological flow regimes in the watersheds of the northeastern U.S. for different thresholds of global temperature increase (1.5, 2.0 and 3.0 °C). Specifically, we examined eight watersheds in the NEUS with different land uses and land covers to explore how anthropogenic activities will have an impact on different quantiles of streamflow conditions (mean, low and peak flows) as well as precipitation in the future under the most extreme GHG emission scenario, RCP8.5. The results show large uncertainties regarding hydrologic regime changes under 1.5 and 2.0 °C temperature increases. However, it was found that streamflow regimes are likely to change for the majority of the watersheds under a 3.0 °C temperature increase. The results indicate that most of the watersheds in the future will enter a wetter regime, particularly during the months of winter, which will be driven by increased seasonal precipitation. In addition, future streamflow projections also suggest a drier fall season for most of the basins due to a lack of precipitation and increase in consecutive dry days in the region.

This study utilizes multiple GCM projections to account for uncertainties that may arise from meteorological inputs. However, hydrological uncertainties remain unaccounted for in this study since we used a single hydrological model to obtain future streamflow projections. Hydrological models are simplified representations of many physical processes, and currently, there exists no perfect model that can accurately capture these physical processes to predict runoff or streamflow. Thus, using a different hydrological model may give us a different result which should also be further investigated. Additionally, uncertainties can also stem from sources such as meteorological downscaling, hydrologic model parameters (e.g., land use changes), etc. In future studies, therefore, we recommend addressing the above-mentioned uncertainties to ensure more robust model outcomes. Despite the limitations, this study can provide useful information for local policy makers and stakeholders to set up plans for restricting GHG emissions and making future climate change adaptations.

**Author Contributions:** Conceptualization, R.S. and R.N.P.; methodology, R.S.; software, R.S.; validation, R.S., A.M. and N.M.; formal analysis, R.S.; investigation, R.S.; resources, R.N.P.; data curation, R.S.; writing—original draft preparation, R.S.; writing—review and editing, A.M., N.M.; visualization, R.S., R.N.P.; supervision, R.N.P.; project administration, R.N.P.; funding acquisition, R.S. All authors have read and agreed to the published version of the manuscript.

**Funding:** This research received no external funding.

**Data Availability Statement:** The data that support the findings of this study are available from the corresponding author upon reasonable request.

**Acknowledgments:** The first author is thankful to Ambarish Karmalkar for providing some of the climate data and consultation.

**Conflicts of Interest:** The authors declare no conflict of interest.

## References

1. Hirabayashi, Y.; Mahendran, R.; Koirala, S.; Konoshima, L.; Yamazaki, D.; Watanabe, S.; Kim, H.; Kanae, S. Global flood risk under climate change. *Nat. Clim. Chang.* **2013**, *3*, 816–821. [[CrossRef](#)]
2. Milly, P.C.D.; Wetherald, R.T.; Dunne, K.A.; Delworth, T.L. Increasing risk of great floods in a changing climate. *Nature* **2002**, *415*, 514–517. [[CrossRef](#)] [[PubMed](#)]
3. Qin, Y.; Abatzoglou, J.T.; Siebert, S.; Huning, L.S.; AghaKouchak, A.; Mankin, J.S.; Hong, C.; Tong, D.; Davis, S.J.; Mueller, N.D. Agricultural risks from changing snowmelt. *Nat. Clim. Chang.* **2020**, *10*, 459–465. [[CrossRef](#)]
4. Blöschl, G.; Hall, J.; Parajka, J.; Perdigão, R.A.P.; Merz, B.; Arheimer, B.; Aronica, G.T.; Bilibashi, A.; Bonacci, O.; Borga, M.; et al. Changing climate shifts timing of European floods. *Science* **2017**, *357*, 588–590. [[CrossRef](#)]
5. Van Loon, A.F. Hydrological drought explained. *WIREs Water* **2015**, *2*, 359–392. [[CrossRef](#)]

6. Hayhoe, K.; Wake, C.P.; Huntington, T.G.; Luo, L.; Schwartz, M.D.; Sheffield, J.; Wood, E.; Anderson, B.; Bradbury, J.; DeGaetano, A.; et al. Past and future changes in climate and hydrological indicators in the US Northeast. *Clim. Dyn.* **2007**, *28*, 381–407. [\[CrossRef\]](#)
7. Siddique, R.; Karmalkar, A.; Fengyun., S.; Palmer, R.N. Hydrological extremes across the Commonwealth of Massachusetts. *J. Hydrol. Reg. Stud.* **2020**. Under Review. [\[CrossRef\]](#)
8. Siddique, R.; Palmer, R. Climate Change Impacts on Local Flood Risks in the U.S. Northeast: A Case Study on the Connecticut and Merrimack River Basins. *JAWRA J. Am. Water Resour. Assoc.* **2020**. [\[CrossRef\]](#)
9. Campbell, J.L.; Driscoll, C.T.; Pourmokhtarian, A.; Hayhoe, K. Streamflow responses to past and projected future changes in climate at the Hubbard Brook Experimental Forest, New Hampshire, United States. *Water Resour. Res.* **2011**, *47*, W02514. [\[CrossRef\]](#)
10. Betsill, M.; Dubash, N.K.; Paterson, M.; van Asselt, H.; Vihma, A.; Winkler, H. Building productive links between the UNFCCC and the broader global climate governance landscape. *Glob. Environ. Politics* **2015**, *15*, 1–10. [\[CrossRef\]](#)
11. Rogelj, J.; den Elzen, M.; Höhne, N.; Fransen, T.; Fekete, H.; Winkler, H.; Schaeffer, R.; Sha, F.; Riahi, K.; Meinshausen, M. Paris Agreement climate proposals need a boost to keep warming well below 2 °C. *Nature* **2016**, *534*, 631. [\[CrossRef\]](#) [\[PubMed\]](#)
12. Friedlingstein, P.; Andrew, R.M.; Rogelj, J.; Peters, G.P.; Canadell, J.G.; Knutti, R.; Luderer, G.; Raupach, M.R.; Schaeffer, M.; van Vuuren, D.P.; et al. Persistent growth of CO<sub>2</sub> emissions and implications for reaching climate targets. *Nat. Geosci.* **2014**, *7*, 709. [\[CrossRef\]](#)
13. Gosling, S.N.; Zaherpour, J.; Mount, N.J.; Hattermann, F.F.; Dankers, R.; Arheimer, B.; Breuer, L.; Ding, J.; Haddeland, I.; Kumar, R. A comparison of changes in river runoff from multiple global and catchment-scale hydrological models under global warming scenarios of 1 C, 2 C and 3 C. *Clim. Chang.* **2017**, *141*, 577–595. [\[CrossRef\]](#)
14. Demaria, E.M.C.; Palmer, R.N.; Roundy, J.K. Regional climate change projections of streamflow characteristics in the Northeast and Midwest U.S. *J. Hydrol. Reg. Stud.* **2016**, *5*, 309–323. [\[CrossRef\]](#)
15. Marshall, E.; Randhir, T. Effect of climate change on watershed system: A regional analysis. *Clim. Chang.* **2008**, *89*, 263–280. [\[CrossRef\]](#)
16. Parr, D.; Wang, G.; Ahmed, K.F. Hydrological changes in the U.S. Northeast using the Connecticut River Basin as a case study: Part 2. Projections of the future. *Glob. Planet. Chang.* **2015**, *133*, 167–175. [\[CrossRef\]](#)
17. Parr, D.; Wang, G. Hydrological changes in the U.S. Northeast using the Connecticut River Basin as a case study: Part 1. Modeling and analysis of the past. *Glob. Planet. Chang.* **2014**, *122*, 208–222. [\[CrossRef\]](#)
18. Mitchell, D.; James, R.; Forster, P.M.; Betts, R.A.; Shiogama, H.; Allen, M. Realizing the impacts of a 1.5 C warmer world. *Nat. Clim. Chang.* **2016**, *6*, 735. [\[CrossRef\]](#)
19. Barnett, T.P.; Adam, J.C.; Lettenmaier, D.P. Potential impacts of a warming climate on water availability in snow-dominated regions. *Nature* **2005**, *438*, 303. [\[CrossRef\]](#)
20. Leng, G.; Huang, M.; Voisin, N.; Zhang, X.; Asrar, G.R.; Leung, L.R. Emergence of new hydrologic regimes of surface water resources in the conterminous United States under future warming. *Environ. Res. Lett.* **2016**, *11*, 114003. [\[CrossRef\]](#)
21. Marx, A.; Kumar, R.; Thober, S.; Rakovec, O.; Wanders, N.; Zink, M.; Wood, E.F.; Pan, M.; Sheffield, J.; Samaniego, L. Climate change alters low flows in Europe under global warming of 1.5, 2, and 3° C. *Hydrol. Earth Syst. Sci.* **2018**, *22*, 1017–1032. [\[CrossRef\]](#)
22. Taylor, K.E.; Stouffer, R.J.; Meehl, G.A. An overview of CMIP5 and the experiment design. *Bull. Am. Meteorol. Soc.* **2012**, *93*, 485–498. [\[CrossRef\]](#)
23. Meinshausen, M.; Smith, S.J.; Calvin, K.; Daniel, J.S.; Kainuma, M.L.T.; Lamarque, J.-F.; Matsumoto, K.; Montzka, S.A.; Raper, S.C.B.; Riahi, K. The RCP greenhouse gas concentrations and their extensions from 1765 to 2300. *Clim. Chang.* **2011**, *109*, 213. [\[CrossRef\]](#)
24. Karmalkar, A.V.; Thibeault, J.M.; Bryan, A.M.; Seth, A. Identifying credible and diverse GCMs for regional climate change studies—case study: Northeastern United States. *Clim. Change* **2019**, *154*, 367–386. [\[CrossRef\]](#)
25. Pierce, D.W.; Cayan, D.R.; Thrasher, B.L. Statistical downscaling using localized constructed analogs (LOCA). *J. Hydrometeorol.* **2014**, *15*, 2558–2585. [\[CrossRef\]](#)
26. Zhang, J.; Howard, K.; Langston, C.; Vasiloff, S.; Kaney, B.; Arthur, A.; Van Cooten, S.; Kelleher, K.; Kitzmiller, D.; Ding, F. National Mosaic and Multi-Sensor QPE (NMQ) system: Description, results, and future plans. *Bull. Am. Meteorol. Soc.* **2011**, *92*, 1321–1338. [\[CrossRef\]](#)
27. Prat, O.P.; Nelson, B.R. Evaluation of precipitation estimates over CONUS derived from satellite, radar, and rain gauge data sets at daily to annual scales (2002–2012). *Hydrol. Earth Syst. Sci.* **2015**, *19*, 2037. [\[CrossRef\]](#)
28. Seo, D.-J.; Siddique, R.; Ahnert, P. Objective reduction of rain gauge network via geostatistical analysis of uncertainty in radar-gauge precipitation estimation. *J. Hydrol. Eng.* **2015**, *20*. [\[CrossRef\]](#)
29. Siddique, R.; Mejia, A.; Brown, J.; Reed, S.; Ahnert, P. Verification of precipitation forecasts from two numerical weather prediction models in the Middle Atlantic Region of the USA: A precursory analysis to hydrologic forecasting. *J. Hydrol.* **2015**, *529*. [\[CrossRef\]](#)
30. Yang, X.; Sharma, S.; Siddique, R.; Greybush, S.J.; Mejia, A. Postprocessing of GEFS precipitation ensemble reforecasts over the U.S. mid-atlantic region. *Mon. Weather Rev.* **2017**, *145*. [\[CrossRef\]](#)
31. James, R.; Washington, R.; Schleussner, C.-F.; Rogelj, J.; Conway, D. Characterizing half-a-degree difference: A review of methods for identifying regional climate responses to global warming targets. *WIREs Clim. Chang.* **2017**, *8*, e457. [\[CrossRef\]](#)

32. Fischer, E.M.; Knutti, R. Anthropogenic contribution to global occurrence of heavy-precipitation and high-temperature extremes. *Nat. Clim. Chang.* **2015**, *5*, 560–564. [[CrossRef](#)]
33. Swain, S.; Hayhoe, K. CMIP5 projected changes in spring and summer drought and wet conditions over North America. *Clim. Dyn.* **2015**, *44*, 2737–2750. [[CrossRef](#)]
34. Karmalkar, A.V.; Bradley, R.S. Consequences of Global Warming of 1.5 °C and 2 °C for Regional Temperature and Precipitation Changes in the Contiguous United States. *PLoS ONE* **2017**, *12*, e0168697. [[CrossRef](#)] [[PubMed](#)]
35. Koren, V.; Reed, S.; Smith, M.; Zhang, Z.; Seo, D.-J. Hydrology laboratory research modeling system (HL-RMS) of the US national weather service. *J. Hydrol.* **2004**, *291*, 297–318. [[CrossRef](#)]
36. Koren, V.; Smith, M.; Cui, Z. Physically-based modifications to the Sacramento Soil Moisture Accounting model. Part A: Modeling the effects of frozen ground on the runoff generation process. *J. Hydrol.* **2014**, *519*, 3475–3491. [[CrossRef](#)]
37. Siddique, R.; Mejia, A. Ensemble Streamflow Forecasting across the US Mid-Atlantic Region with a Distributed Hydrological Model Forced by GEF5 Reforecasts. *J. Hydrometeorol.* **2017**, *18*, 1905–1928. [[CrossRef](#)]
38. Wood, A.W.; Hopson, T.; Newman, A.; Brekke, L.; Arnold, J.; Clark, M. Quantifying streamflow forecast skill elasticity to initial condition and climate prediction skill. *J. Hydrometeorol.* **2016**, *17*, 651–668. [[CrossRef](#)]
39. Sharma, S.; Siddique, R.; Reed, S.; Ahnert, P.; Mendoza, P.; Mejia, A. Relative effects of statistical preprocessing and postprocessing on a regional hydrological ensemble prediction system. *Hydrol. Earth Syst. Sci.* **2018**, *22*. [[CrossRef](#)]
40. Burnash, R.J.C. The NWS river forecast system-catchment modeling. *Comput. Model. Watershed Hydrol.* **1995**, *188*, 311–366.
41. Armstrong, D.S.; Parker, G.W.; Richards, T.A. *Characteristics and Classification of least Altered Streamflows in Massachusetts*; US Department of the Interior, US Geological Survey: Reston, VA, USA, 2008; ISBN 141132188X.
42. Archfield, S.; Vogel, R.; Steeves, P.; Brandt, S.; Weiskel, P.; Garabedian, S. The Massachusetts Sustainable-Yield Estimator: A decision-support tool to assess water availability at ungaged sites in Massachusetts. *US Geol. Surv. Sci. Investig. Rep.* **2009**, *5227*, 2010.
43. Kuzmin, V.; Seo, D.-J.; Koren, V. Fast and efficient optimization of hydrologic model parameters using a priori estimates and stepwise line search. *J. Hydrol.* **2008**, *353*, 109–128. [[CrossRef](#)]
44. Deser, C.; Knutti, R.; Solomon, S.; Phillips, A.S. Communication of the role of natural variability in future North American climate. *Nat. Clim. Chang.* **2012**, *2*, 775–779. [[CrossRef](#)]
45. Fyfe, J.C.; Gillett, N.P.; Zwiers, F.W. Overestimated global warming over the past 20 years. *Nat. Clim. Chang.* **2013**, *3*, 767–769. [[CrossRef](#)]
46. Hawkins, E.; Sutton, R. The potential to narrow uncertainty in projections of regional precipitation change. *Clim. Dyn.* **2011**, *37*, 407–418. [[CrossRef](#)]
47. Hawkins, E.; Sutton, R. The potential to narrow uncertainty in regional climate predictions. *Bull. Am. Meteorol. Soc.* **2009**, *90*, 1095–1108. [[CrossRef](#)]
48. Hawkins, E.; Sutton, R. Time of emergence of climate signals. *Geophys. Res. Lett.* **2012**, *39*. [[CrossRef](#)]
49. Giorgi, F.; Bi, X. Time of emergence (TOE) of GHG-forced precipitation change hot-spots. *Geophys. Res. Lett.* **2009**, *36*. [[CrossRef](#)]
50. Zhuan, M.-J.; Chen, J.; Shen, M.-X.; Xu, C.-Y.; Chen, H.; Xiong, L.-H. Timing of human-induced climate change emergence from internal climate variability for hydrological impact studies. *Hydrol. Res.* **2018**, *49*, 421–437. [[CrossRef](#)]